Journal of the Mechanics and Physics of Solids 61 (2013) 611–628

Contents lists available at SciVerse ScienceDirect

Journal of the Mechanics and Physics of Solids

journal homepage: www.elsevier.com/locate/jmps

Giant voltage-induced deformation in dielectric elastomers near the verge of snap-through instability

Tiefeng Li [a,b,c], Christoph Keplinger [c,d], Richard Baumgartner [d], Siegfried Bauer [d], Wei Yang [a], Zhigang Suo [c,*]

[a] Institute of Applied Mechanics, Zhejiang University, 38 Zheda Road, Hangzhou, Zhejiang 310027, China
[b] Soft Matter Research Center (SMRC), Zhejiang University, Hangzhou 310027, China
[c] School of Engineering and Applied Sciences, Kavli Institute for Bionano Science and Technology, Harvard University, Cambridge, MA 02138, USA
[d] Soft Matter Physics, Johannes Kepler University, Altenbergerstrasse 69, A-4040 Linz, Austria

ARTICLE INFO

Article history:
Received 9 January 2012
Received in revised form
13 June 2012
Accepted 2 September 2012
Available online 23 September 2012

Keywords:
Dielectric elastomer
Finite strain
Snap-through instability
Bifurcation
Electromechanical processes

ABSTRACT

Dielectric elastomers are capable of large voltage-induced deformation, but achieving such large deformation in practice has been a major challenge due to electromechanical instability and electric breakdown. The complex nonlinear behavior suggests an important opportunity: electromechanical instability can be harnessed to achieve giant voltage-induced deformation. We introduce the following principle of operation: place a dielectric elastomer near the verge of snap-through instability, trigger the instability with voltage, and bend the snap-through path to avert electric breakdown. We demonstrate this principle of operation with a commonly used experimental setup—a dielectric membrane mounted on a chamber of air. The behavior of the membrane can be changed dramatically by varying parameters such as the initial pressure in the chamber, the volume of the chamber, and the prestretch of the membrane. We use a computational model to analyze inhomogeneous deformation and map out bifurcation diagrams to guide the experiment. With suitable values of the parameters, we obtain giant voltage-induced expansion of area by 1692%, far beyond the largest value reported in the literature.

1. Introduction

Dielectric elastomers are being developed as artificial muscles for diverse applications, including soft machines, adaptive optics, haptic surfaces, and energy harvesting (Brochu and Pei, 2010; Carpi et al., 2010; Kornbluh et al., 2012). Desirable attributes include large voltage-induced deformation, high energy density, fast response, quiet operation, light weight, and low cost. In such an artificial muscle, a membrane of a dielectric elastomer is sandwiched between two compliant electrodes typically made of carbon grease (Fig. 1). When the electrodes are subject to a voltage, electrons flow through the external circuit from one electrode to the other. Charges of opposite signs on the two electrodes attract each other, so that the membrane reduces its thickness and expands its area. The dielectric elastomer enables electromechanical transduction: the voltage can deform the membrane, and the deformation changes the capacitance of the membrane.

Large voltage-induced deformation gives dielectric elastomers a competitive edge over other active materials. Reported voltage-induced strains have increased from a linear strain of 4% with polyurethane (Ma et al., 1994), to about 30% with

* Corresponding author.
E-mail address: suo@seas.harvard.edu (Z. Suo).

0022-5096/$ - see front matter © 2012 Elsevier Ltd. All rights reserved.
http://dx.doi.org/10.1016/j.jmps.2012.09.006

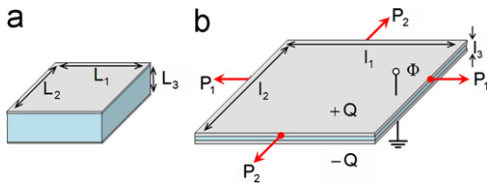

Fig. 1. A membrane of a dielectric elastomer is sandwiched between two compliant electrodes. (a) In the reference state, the membrane is subject to neither force nor voltage, and is undeformed. (b) In the activated state, the membrane is subjected to biaxial forces, and the two electrodes are subject to voltage.

silicone (Pelrine et al., 1998), and to over 100% with a prestretched acrylic elastomer (Pelrine et al., 2000). Reliably inducing large deformation by voltage, however, has remained a major challenge in practice. Deformable elastomers are susceptible to electromechanical instability (Stark and Garton, 1955). As the voltage is ramped up, the membrane thins down and the electric field amplifies, often leading to pull-in instability, followed by electric breakdown (Zhao and Suo, 2007; Norris, 2008). On the other hand, when charges are sprayed on a dielectric membrane with no electrodes, electromechanical instability is removed and extremely large deformation is achievable (Keplinger et al., 2010; Li et al., 2011). The lack of electrodes in this setup, however, limits its scope of application.

Electromechanical instability is affected by both material models and boundary conditions (e.g., Zhao et al., 2007; Diaz-Calleja et al., 2008; Leng et al., 2009; De Tommasi et al., 2010; Xu et al., 2010; Bertoldi and Gei, 2011; Rudykh, et al., 2012; Yong et al., 2012). Consequently, achievable voltage-induced deformation is not an intrinsic property of a material, but is a property of a structure that can be markedly affected by boundary conditions. For example, voltage-induced deformation is enhanced when a membrane is prestretched and constrained by a rigid ring (Pelrine et al., 2000; Wissler and Mazza, 2005a), and is further enhanced when the membrane is subject to equal-biaxial dead load (Koh et al., 2011b; Huang et al., 2012). By contrast, voltage-induced deformation is reduced when the membrane is subject to uniaxial dead load (Huang and Suo, 2012; Lu et al., 2012). Furthermore, Kollosche et al. (2012) show that a relatively simple setup—a membrane prestretched with two rigid clamps and a dead load—displays remarkably complex interplay of nonlinear processes, including local instability, wrinkling, and snap-through instability. The setup gives drastically different values of voltage-induced deformation, depending on the state of prestretches.

The complex nonlinear behavior suggests an important opportunity: electromechanical instability may be harnessed to achieve giant voltage-induced deformation (Mockensturm and Goulbourne, 2006; Goulbourne et al., 2007; Zhao and Suo, 2010). Rather than causing failure, the instability can be a feature. As an example, we have recently introduced the following principle of operation: place a dielectric elastomer in a state near the verge of snap-through instability, trigger the instability with a voltage, and bend the snap-through path to avert electric breakdown (Keplinger et al., 2012). We have demonstrated the principle of operation with a dielectric membrane mounted on a chamber (Fig. 2)—a setup commonly used to study electromechanical coupling of dielectric elastomers (e.g., Fox and Goulbourne, 2008; Rosset et al., 2009). When air is pumped into the chamber through a valve, the membrane is inflated into a balloon. The valve is subsequently closed to fix the amount of air enclosed by the chamber and balloon. When voltage is applied between the two carbon-grease electrodes, the balloon expands further. With an acrylic elastomer (3M™VHB™4910), we have demonstrated voltage-induced expansion of area by 1692%, well beyond the largest value of 380% reported before (Pelrine et al., 2000).

While our previous paper (Keplinger et al., 2012) has described the principle of operation and the experimental demonstration, the present paper reports theoretical analysis and further experimental observations. We use a computational model that combines the nonlinear electromechanical coupling of the material and the kinematics of large deformation of the membrane. In numerical simulation, care is taken to capture inhomogeneous and large deformation, as well as highly nonlinear behavior of the snap-through instability. We calculate bifurcation diagrams to map out multiple branches of solutions as the parameters of the setup vary. For example, we show that the behavior of the membrane is dramatically affected by varying the volume of the chamber. When the chamber is too small, the pressure drops steeply as the membrane is actuated by the voltage, and the achievable voltage-induced deformation is small. When the chamber is too large, the pressure is nearly constant as the membrane is actuated by the voltage, and the membrane snaps into an excessively large balloon, failed by electric breakdown before it reaches a stable state. When the chamber is of an intermediate size, the pressure drops somewhat as the membrane is actuated by the voltage, and the membrane snaps to a stable state of a large volume, averting electric breakdown. We compare these theoretical predictions with experimental observations. We further present experimental observations of voltage-induced local instability and clefts.

The VHB dielectric elastomer used in our experiments has been widely employed due to its large stretchability and high electric breakdown strength. The material, however, exhibits pronounced viscoelasticity (Lochmatter et al., 2007; Plante and Dubowsky, 2007). While a nonlinear viscoelastic model for dielectric elastomers has been proposed (Hong, 2011; Zhao et al., 2011; Foo et al., 2012), the model has not been reliably calibrated for the VHB. Here we will adopt a nonlinear elastic model. The object is to use numerical simulations to guide the experiment, rather than to achieve an exact match with the experiment. To reduce the effect of viscoelasticity in the experiment, we will use low voltage ramping rates. While such low ramping rates will not be interesting for the majority of projected applications, the combined model and experiment shed light on large voltage-induced deformation. It is also anticipated that less viscoelastic materials, such as natural rubber and PDMS, will be developed to function as dielectric elastomers.

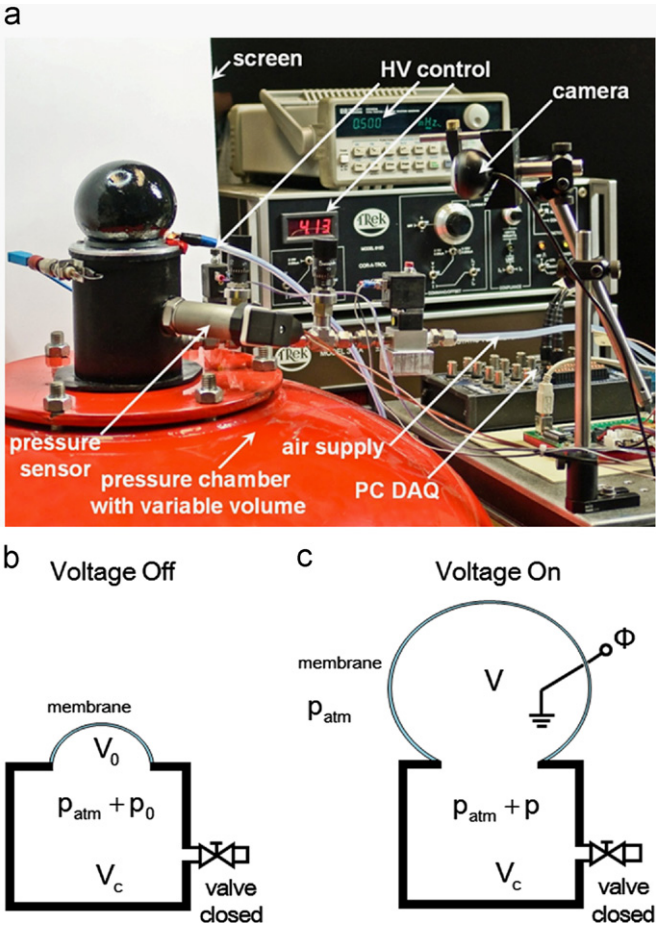

Fig. 2. Experimental setup. (a) A dielectric membrane of 3M™VHB™4910, initial thickness 1 mm, is sandwiched between two carbon-grease electrodes. The membrane is mounted on a chamber of circular opening, radius 22.5 mm. (b) When air is pumped into the chamber through a valve, the membrane is inflated into a balloon. Subsequently, the valve is closed to fix the amount of air enclosed by the chamber and balloon. (c) When voltage is applied between the two carbon-grease electrodes, the balloon expands further.

The paper is organized as follows. Section 2 described a material model of nonlinear electromechanical coupling, with material constants specified in Section 3. Section 4 recalls field equations in elasticity and electrostatics. Section 5 describes a method to calculate inhomogeneous deformation and bifurcation diagrams. Section 6 presents numerical simulations that explore how to vary parameters to achieve giant voltage-induced deformation. Section 7 reports experimental observations.

2. Homogeneous state

Along with the rapid advances in developing dielectric elastomers, the nonlinear field theory of deformable dielectrics has gained renewed attention (e.g., Dorfmann and Ogden, 2005; McMeeking and Landis, 2005; Goulbourne et al., 2005; Wissler and Mazza, 2005a; Vu et al., 2007; Suo et al., 2008; O'Brien et al., 2009; Trimarco, 2009). The theory has a remarkably simple structure: fundamental field equations are identical to those in elasticity and electrostatics, while electromechanical coupling enters the theory exclusively from material models. In the field theory, material models are formulated using homogeneous states. For a review of the nonlinear field theory, see Suo (2010).

A material model to be used here is specified in this section. Fig. 1 illustrates a membrane of a dielectric elastomer sandwiched between two compliant electrodes. In the reference state, the membrane is subject to neither force nor voltage, and is of dimensions L_1, L_2 and L_3. In a homogeneous state in which the membrane is subject to forces P_1 and P_2 and the two electrodes are subject to voltage Φ through a conducting wire, the dimensions of the membrane become l_1, l_2 and l_3, and a quantity of charge Q goes through the conducting wire from one electrode to the other. Define the stretches by $\lambda_1=l_1/L_1$, $\lambda_2=l_2/L_2$ and $\lambda_3=l_3/L_3$; the stresses by $\sigma_1=P_1/(l_2l_3)$ and $\sigma_2=P_2/(l_1l_3)$; the electric field by $E=\Phi/l_3$; and the electric displacement by $D=Q/(l_1l_2)$.

When an elastomer undergoes large deformation, the change in the shape of the elastomer is typically much larger than the change in the volume of the elastomer. As an idealization, the elastomer is taken to be incompressible:

$$\lambda_1\lambda_2\lambda_3 = 1, \tag{1}$$

this idealization places a constraint among the three stretches. We regard λ_1 and λ_2 as independent variables.

To construct a material model, recall the molecular picture of an elastomer—a network of polymers held together by crosslinks. Each polymer is a chain of many links, and each link is either a polar or a nonpolar molecular group. At a finite temperature, the network fluctuates among many configurations: the neighboring links may rotate relative to each other, and the polarization of each link may also rotate and change magnitude. Subject to a force and voltage, the elastomer deforms and polarizes in certain directions.

For a polymer chain of many links, when the applied force and voltage are not too large, the end-to-end distance of each polymer chain is much smaller than the contour length of the chain. Consequently, the deformation of the polymer chain negligibly affects the polarization of the individual links. As an idealization, it is commonly assumed that the dielectric behavior of an elastomer is exactly the same as that of a polymer melt, independent of deformation:

$$D = \varepsilon E, \tag{2}$$

where ε is the permittivity of the elastomer, taken to be a constant independent of deformation and electric displacement. This idealization is known as the model of ideal dielectric elastomers (Zhao et al., 2007), and is consistent with the following experimental observation: the permittivity changes negligibly when the membrane is stretched 25 times its initial area (Kofod et al., 2003).

For an ideal dielectric elastomer, the stress–stretch relations take the form:

$$\sigma_1 + \varepsilon E^2 = \lambda_1 \frac{\partial W_{\text{stretch}}(\lambda_1,\lambda_2)}{\partial \lambda_1}, \tag{3}$$

$$\sigma_2 + \varepsilon E^2 = \lambda_2 \frac{\partial W_{\text{stretch}}(\lambda_1,\lambda_2)}{\partial \lambda_2}, \tag{4}$$

where $W_{\text{stretch}}(\lambda_1,\lambda_2)$ is the free energy associated with the stretching of the elastomer. The deformation due to the electric field applied through the thickness of a membrane is the same as the deformation caused by equal-biaxial tensile stresses of magnitude εE^2, called the Maxwell stresses. Because the elastomer is taken to be incompressible, the deformation caused by the equal biaxial tensile stresses applied in the plane of the membrane is the same as that caused by a uniaxial compressive stress applied through the thickness of the membrane. The model of ideal dielectric elastomer has been used almost exclusively in the literature (e.g., Wissler and Mazza, 2005a; Goulbourne et al., 2005; Plante and Dubowsky, 2006). See also Zhao and Suo (2008) and Li et al. (2012) for models of non-ideal dielectric elastomers.

We choose a specific form of the free-energy function on the basis of the following consideration. Upon approaching a limiting stretch due to the finite contour length of the polymer chains, the elastomer stiffens steeply, which can greatly affect electromechanical instability. To account for stiffening, we adopt the Gent (1996) model:

$$W_{\text{stretch}} = -\frac{\mu J_{\text{lim}}}{2}\log\left(1 - \frac{\lambda_1^2+\lambda_2^2+\lambda_3^2-3}{J_{\text{lim}}}\right), \tag{5}$$

where μ is the shear modulus, and J_{lim} a constant related to the limiting stretch. The stretches satisfy $0 \le (\lambda_1^2+\lambda_2^2+\lambda_3^2-3)/J_{\text{lim}} < 1$. When $(\lambda_1^2+\lambda_2^2+\lambda_3^2-3)/J_{\text{lim}} \to 0$, the Taylor expansion of (5) gives that gives $W_{\text{stretch}} \to \mu(\lambda_1^2+\lambda_2^2+\lambda_3^2-3)/2$. That is, the Gent model recovers the neo-Hookean model when deformation is small compared to the limiting stretch. When $(\lambda_1^2+\lambda_2^2+\lambda_3^2-3)/J_{\text{lim}} \to 1$, the elastomer approaches the limiting stretch. For example, under equal-biaxial stresses, $\lambda_1=\lambda_2=\lambda$ and $\lambda_3=\lambda^{-2}$, so that the limiting stretch λ_{lim} is given by $J_{\text{lim}} = 2\lambda_{\text{lim}}^2 + \lambda_{\text{lim}}^{-4} - 3$.

Inserting (5) into (3) and (4), we obtain that

$$\sigma_1 + \varepsilon E^2 = \frac{\mu(\lambda_1^2-\lambda_3^2)}{1-(\lambda_1^2+\lambda_2^2+\lambda_3^2-3)/J_{\text{lim}}}, \tag{6}$$

$$\sigma_2 + \varepsilon E^2 = \frac{\mu(\lambda_2^2-\lambda_3^2)}{1-(\lambda_1^2+\lambda_2^2+\lambda_3^2-3)/J_{\text{lim}}}, \tag{7}$$

Eqs. (1), (2), (6) and (7) are the equations of state for incompressible, ideal dielectric elastomers with the Gent free energy of stretching.

3. Material constants

Wissler and Mazza (2005b) have fitted experimentally measured stress–stretch curves of the VHB to the eight-chain model (Arruda and Boyce, 1993), giving the shear modulus $\mu = 68$ kPa and the number of links per chain $n = 125$. The eight-chain model is known to exhibit similar behavior as the Gent model (Boyce, 1996). Fig. 3a shows that the eight-chain model of $\mu = 68$ kPa and $n = 125$ corresponds well with the Gent model of $\mu = 68$ kPa and $J_{\text{lim}} = 372$.

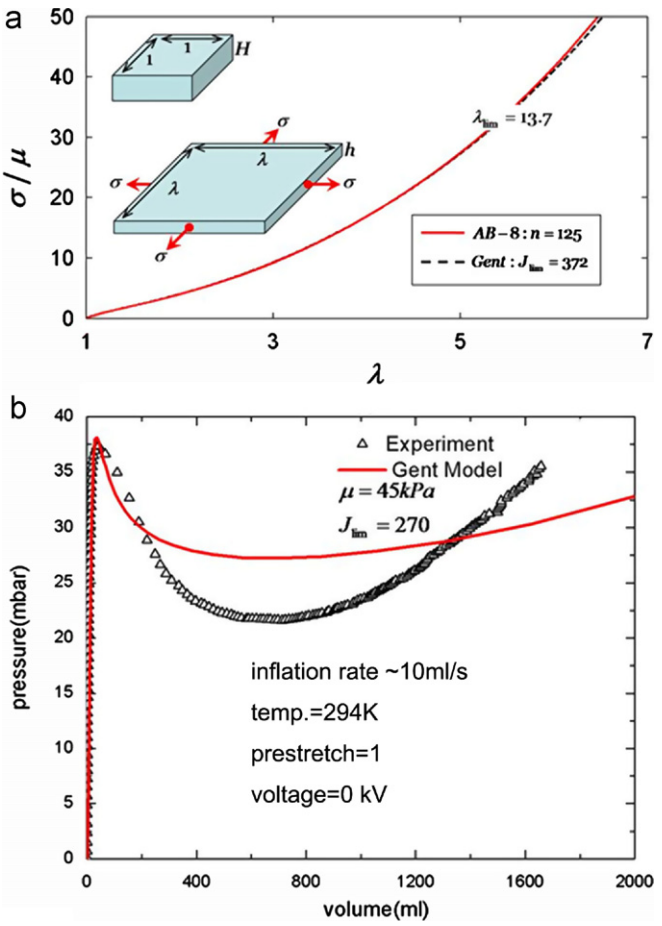

Fig. 3. (a) The membrane stiffens on approaching the limiting stretch associated with the contour length of the polymer chains. This behavior is captured by both the Gent model and the Arruda-Boyce eight-chain model. (b) Comparison of the model and experiment for the pressure–volume curve for a membrane mounted on a chamber.

Using the material model, along with the field equations to be described in Section 4, one can numerically simulate the inflation of a membrane. It has been difficult, however, to achieve quantitative agreement between the numerical simulation and experimentally observed behavior of the inflating membrane (Klingbeil and Shield, 1964). For example, Fig. 3b plots the pressure–volume curve for a membrane in the absence of voltage. When compared with the numerical predictions from the Gent model, the difference between the experimental data and theoretical prediction becomes large after the peak pressure. The disagreement is still evident when we try to fit the numerical simulation to experimental data by adjusting both μ and $J_{\lim}$. We have adjusted the parameters to $\mu=45$ kPa and $J_{\lim}=270$ in comparing the experiment and the model (Fig. 3b). The disagreement between the experiment and the model may be interpreted as follows. First, a two-parameter model such as the Gent model or the Arruda-Boyce model may not adequately represent the stress–stretch behavior of the VHB. Second, the VHB exhibits pronounced viscoelasticity, which is not captured by the numerical simulation on the basis of elastic behavior.

These complications aside, Fig. 3b indicates accurate prediction of the peak pressure and trend after the peak. A qualitative analysis based on the Gent model seems to be feasible to reveal the snap-through instability. In the subsequent analyses, with this simplification in mind, we will use the Gent model with $\mu=45$ kPa and $J_{\lim}=270$. We will use the numerical simulation to guide the design of the experiment, and will not make quantitative comparison between simulation and experiment.

The permittivity is commonly written as $\varepsilon=\varepsilon_0\varepsilon_r$, where $\varepsilon_0=8.854\times10^{-12}$ F/m is the permittivity of the vacuum, and ε_r the relative permittivity. For 3M™VHB™4910, Kofod et al. (2003) reported a value of $\varepsilon_r=4.7$.

Dielectric elastomers typically fail by electric breakdown. Electric breakdown is a poorly understood phenomenon. In this paper, we proceed as follows. Experimental data for VHB show that the critical field for electric breakdown, E_{EB}, increases with stretch (Kofod et al., 2003; Plante and Dubowsky, 2006). The experimental data are fit to the form Koh et al. (2011a):

$$E_{EB}=\begin{cases}30.6\lambda^{1.13}\ \text{MV}/m, & \text{for}\quad \lambda<5.7\\ 218\ \text{MV}/m, & \text{for}\quad \lambda>5.7\end{cases} \tag{8}$$

the experiments were carried out for membranes under equal-biaxial stretch λ. In analyzing a membrane under unequal-biaxial stretches, $\lambda_1 \neq \lambda_2$, we interpret λ^2 as the area strain, and use (8) by setting $\lambda^2 = \lambda_1\lambda_2$. For a dielectric membrane with inhomogeneous electric field, we assume that the membrane fails when the electric field of any point in the membrane exceeds the electric breakdown field.

4. Inhomogeneous state

When the initially flat membrane expands into a balloon, the state of the membrane becomes inhomogeneous. For example, the apex of the membrane is under equal-biaxial stretches, while the edge of the membrane is under unequal-biaxial stretches. The edge of the membrane is clamped by the chamber; as the membrane expands into a balloon, the latitudinal stretch remains fixed, but the longitudinal stretch changes. The inhomogeneous state of the membrane has been modeled by combining the material model and the field equations (e.g., Goulbourne et al., 2005; Mockensturm and Goulbourne, 2006; He et al., 2009; Zhu et al., 2010; Wang et al., 2012). As mentioned at the beginning of Section 2, the field equations in the theory of deformable dielectrics are identical to those in elasticity and electrostatics. This section recalls these field equations.

Fig. 4 illustrates the cross-section of the membrane in several states. In the reference state (Fig. 4a), the membrane is subject to neither stress nor electric field, and is of flat circular shape, thickness H and radius A. In the reference state, we label each material particle by its distance R from the center of the membrane O. In the prestretched state (Fig. 4b), the membrane is stretched and mounted to a chamber with a circular opening of radius a, the ratio $\lambda_0 = a/A$ being the prestretch in the membrane. In the pressurized state (Fig. 4c), the air outside the balloon is under atmospheric pressure p_{atm}, and the air inside the balloon is subject to pressure $p + p_{\text{atm}}$; the difference, p, is called the differential pressure, or simply the pressure for short. In the actuated state (Fig. 4d), the membrane is subject to both the pressure p and the voltage Φ. The deformation of the membrane is assumed to be axisymmetric. A system of coordinates is set up with the origin coinciding with the center of the membrane. The material particle, distance R from the center when the membrane is in the reference state, occupies a place of coordinates r and z when the membrane is in a deformed state.

4.1. Field equations in elasticity

The field equations in the theory of elasticity of membranes are well established (Adkins and Rivlin, 1952). The two functions, $r(R)$ and $z(R)$, specify the deformation of the membrane. Consider a circle of material particles, radius R when the membrane is in the reference state. In a deformed state, the circle of material particles remain a circle, but is of radius $r(R)$ and height $z(R)$. The deformation causes the latitudinal stretch

$$\lambda_2 = r/R, \tag{9}$$

similarly, consider another circle of material particles, radius $R+dR$ when the membrane is in the reference state. In the deformed state, the circle of material particles remain on a circle, radius $r(R+dR)$ and height $z(R+dR)$. In the reference state, the material particles between the two circles form an annulus of width dR. In the deformed state, these material particles form a circular band of width $\lambda_1 dR$, where λ_1 is the longitudinal stretch. In the deformed state, let $\theta(R)$ be the slope of a membrane at material particle R. The geometry dictates that

$$\frac{dz}{dR} = \lambda_1 \sin\theta, \tag{10}$$

$$\frac{dr}{dR} = \lambda_1 \cos\theta, \tag{11}$$

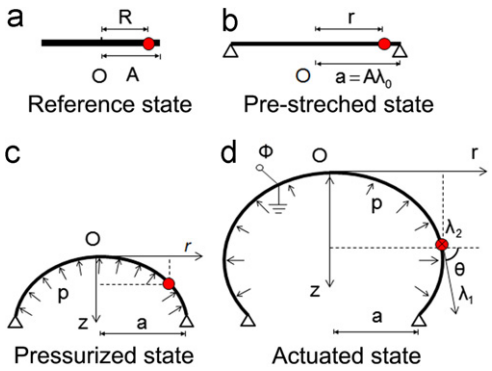

Fig. 4. Cross-section of a dielectric membrane sandwiched between two compliant electrodes. (a) In the reference state, the membrane is of flat circular shape. (b) The membrane is prestretched and held by a rigid ring. (c) Subject to a differential pressure, the membrane inflates out of the plane, and takes an axisymmetric shape. (d) Subject to voltage, the membrane deforms further.

when the membranes are in the prestretched state (Fig. 4b), both stretches are homogeneous in the membrane, $\lambda_1=\lambda_2=\lambda_0$. When the membranes are in a curved state (Fig. 4c and d), however, the stretches are inhomogeneous in the membranes, and are described by functions $\lambda_1(R)$ and $\lambda_2(R)$. Let $h(R)$ be the thickness of the circular band in the deformed state. The membrane is taken to be incompressible, so that

$$h=H/(\lambda_1\lambda_2). \tag{12}$$

The equations that balance forces can be established by using free-body diagrams. In a deformed state (Fig. 4d), the membrane is subject to longitudinal stress $\sigma_1(R)$ and latitudinal stress $\sigma_2(R)$. The geometry of the deformed membrane is described by the thickness $h(R)$, the radius $r(R)$, the height $z(R)$ and the slope $\theta(R)$. Cut a band of the membrane by two planes at z and $z+dz$. Balancing the forces acting on the band and in the z-direction, we obtain that

$$d(\sigma_1 hr\sin\theta)-prdr=0, \tag{13}$$

next cut the band by a plane containing the z-axis. Balancing forces acting on the half band and in the direction normal to the z-axis, we obtain that

$$d(\sigma_1 hr\cos\theta)+prdz-\sigma_2 h\frac{dz}{\sin\theta}=0. \tag{14}$$

4.2. Field equations in electrostatics

The field equations in the electrostatics of membranes take a trivial from. Both faces of the membrane in Fig. 4c are coated with compliant electrodes. When the two electrodes are subject to voltage Φ, the voltage induces in the membrane an electric field:

$$E=\Phi/h, \tag{15}$$

the electric field is in the direction normal to the faces of the membrane. While the voltage Φ is homogeneous, the electric field is inhomogeneous when the thickness of the membrane becomes inhomogeneous. The charge per unit area is given by the electric displacement D. The charge in either electrode is also inhomogeneous.

5. Numerical simulation

The field equations in Section 4, together with the equations of state in Section 2, constitute a model for dielectric membranes. This section briefly describes a numerical method to calculate inhomogeneous deformation and bifurcation diagrams.

Rewrite (13) and (14) to express $d\theta/dR$ and dz/dR explicitly:

$$\frac{d\theta}{dR}=-\frac{\sigma_2\lambda_1}{\sigma_1\lambda_2 R}\sin\theta+\frac{\lambda_1^2\lambda_2 p}{\sigma_1 H}, \tag{16}$$

$$\frac{d\lambda_1}{dR}=\frac{1}{R\frac{\partial(\sigma_1/\lambda_1)}{\partial\lambda_1}}\left(\frac{\sigma_2}{\lambda_2}\cos\theta-\frac{\sigma_1}{\lambda_1}-\frac{\partial(\sigma_1/\lambda_1)}{\partial\lambda_2}(\lambda_1\cos\theta-\lambda_2)\right), \tag{17}$$

the stresses σ_1 and σ_2 are functions of λ_1, λ_2 and E, according to the equations of state (6) and (7).

The four functions $r(R)$, $z(R)$, $\theta(R)$ and $\lambda_1(R)$ are governed by the ordinary differential Eqs. (10), (11), (16) and (17), together with the following boundary conditions. The origin of the coordinates coincides with the apex of the membrane:

$$z(0)=0,\quad r(0)=0, \tag{18}$$

at the apex of the membrane, symmetry dictates that

$$\theta(0)=0, \tag{19}$$

the chamber clamps the edge of the membrane:

$$r(A)=a. \tag{20}$$

We solve the two-point boundary-value problem as an initial-value problem by using the shooting method. The values of all four functions at the apex of the membrane are set as $r(0)=0$, $z(0)=0$, $\theta(0)=0$, $\lambda_1(0)=\lambda_{\text{apex}}$. These values are used as the initial conditions to integrate numerically the ordinary differential Eqs. (10), (11), (16) and (17) to obtain the four functions $r(R)$, $z(R)$, $\theta(R)$ and $\lambda_1(R)$. The value of λ_{apex} is solved to satisfy the boundary condition $r(A)=a$.

Once the four functions $r(R)$, $z(R)$, $\theta(R)$ and $\lambda_1(R)$ are determined, the volume under the membrane is calculated from

$$V=\pi\int_0^R r^2\frac{dz}{dR}dR, \tag{21}$$

the charge on the electrode on either face of the membrane is the electric displacement integrated over the area of the membrane. Recall that $E=\Phi/h=\lambda_1\lambda_2\Phi/H$and $D=\varepsilon E$. In the deformed state, the area of a circular band of the membrane is

$2\pi\lambda_1\lambda_2 RdR$. The magnitude of the charge on either electrode is calculated from

$$Q=\frac{2\pi\varepsilon\Phi}{H}\int_0^R(\lambda_1\lambda_2)^2 RdR, \tag{22}$$

inspecting the governing equations, we note the following dimensionless quantities:

$$\frac{z}{A},\ \frac{r}{A},\ \frac{\sigma}{\mu},\ \frac{D}{\sqrt{\varepsilon\mu}},\ \frac{E}{\sqrt{\mu/\varepsilon}},\ \frac{V}{A^3},\ \frac{p}{\mu H/A},\ \frac{Q}{A^2\sqrt{\varepsilon\mu}},\ \frac{\Phi}{H\sqrt{\mu/\varepsilon}}. \tag{23}$$

Fig. 5 gives an example of the numerical simulation. The membrane is pressurized into a balloon (Fig. 5a). When a voltage is applied in addition to the pressure, the balloon expands to a much larger volume (Fig. 5b). Indicated in Fig. 5b by color is the inhomogeneous electric field in the membrane. The dashed line marks the latitude above which the electric field exceeds the electric breakdown field. Accordingly, at a certain level of the voltage, the membrane should have suffered electric breakdown. Also inhomogeneous in the membrane are the stretches and the stresses (Fig. 5c–f). At a fixed voltage, the longitudinal stretch λ_1 may peak at the apex or an interior point. The latitudinal stretch λ_2 varies monotonically from the maximum at the apex to the minimum at the edge, where the latitudinal stretch is held constant by the rigid ring. Both the longitudinal and latitudinal stresses in the membrane change from the maximum at the apex to the minimum at the edge.

In the absence of voltage, the pressure–volume relation of the membrane is an N-shaped curve—rising, falling, and rising again (Fig. 6a). The curve is calculated by searching for all solutions of the ordinary differential equations for a given value of the pressure, and then repeating the procedure as the pressure is gradually increased. The pressure–volume curve may be regarded as a bifurcation diagram commonly used in nonlinear dynamics (Seydel, 2010). A bifurcation diagram shows how a variable parameter affects states of equilibrium. Here the pressure is a variable parameter, and the volume is a proxy to indicate the state of the membrane—a system of infinite degrees of freedom.

In an experiment in which the pressure is ramped up, when the pressure reaches the peak of the pressure–volume curve, the membrane expands suddenly without appreciable change in the pressure, and attains another stable state of much larger volume. The snap-through expansion of balloons is a subject of many previous studies (e.g., Rivlin and Saunders, 1951; Alexander, 1971; Needleman, 1977; Bogen and McMahon, 1979; Muller and Struchtrup, 2002).

When the membrane is subject to a fixed voltage, the pressure–volume curve lowers somewhat, but still retains the basic shape (Fig. 6a). Using the same procedure, we calculate the voltage–volume curve at a constant pressure (Fig. 6b). For given values of the pressure and voltage, the membrane can be in multiple states of equilibrium (Goulbourne et al., 2005; Mockensturm and Goulbourne, 2006). We may regard the voltage–volume curve as a bifurcation diagram, where the voltage is a variable parameter, and the volume is a proxy to indicate the state of the membrane. Marked in the two figures are several corresponding states: A, B, C and D. Because the pressure–volume curve at $\Phi=0$ is non-monotonic, the curve intersects with the line of a constant pressure—the dashed line in Fig. 6a—at three states of equilibrium. Consequently, the

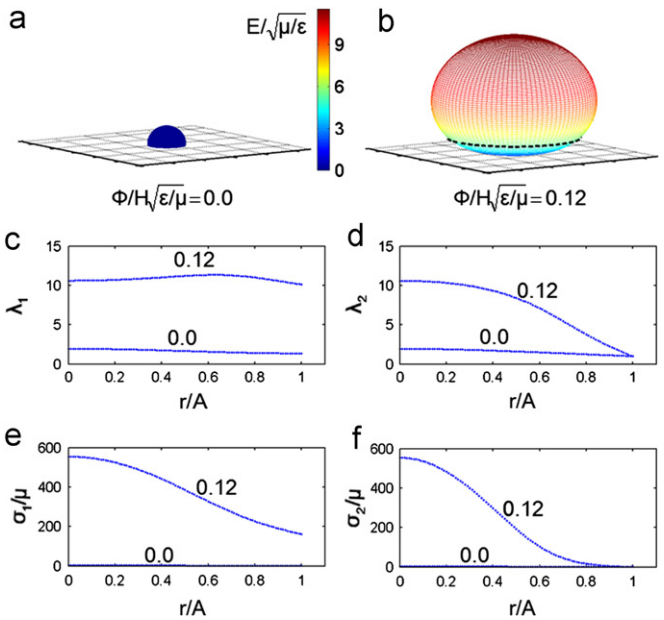

Fig. 5. Numerical results for a membrane subject to pressure of $pA/\mu H=1.82$. (a) The differential pressure inflates the membrane into a balloon. (b) Subject to the differential pressure and the voltage, the balloon expands to a much larger size. The electric field is inhomogeneous in the membrane, and the dashed line marks the latitude above which the electric field exceeds the electric breakdown field. (c–f) Distributions of the stretches and stresses. (For interpretation of the references to color in this figure legend, the reader is referred to the web version of this article.)

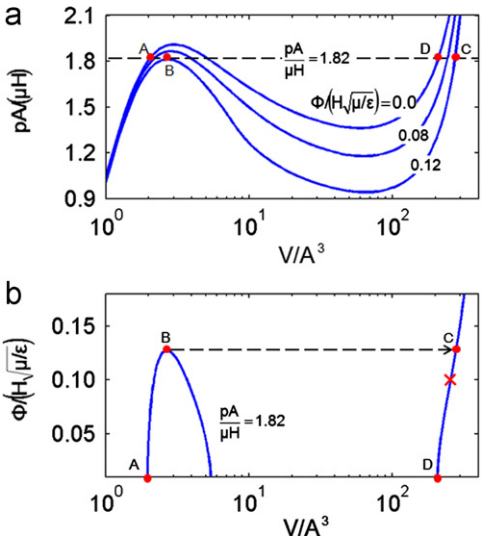

Fig. 6. (a) Pressure–volume curves of a membrane at several values of voltage. (b) Voltage–volume curve of a membrane subject to a constant pressure of $p/(H\mu/A)=1.82$.

voltage–volume curve at the constant value of pressure in Fig. 6b is broken into two parts. Recall that the voltage enters electromechanical coupling as Φ^2: voltages of the opposite signs cause the same deformation.

Next consider an experiment in which the membrane is inflated by pressuring the chamber to state A, near the verge of instability. The pressure is subsequently held constant, and then voltage is switched on and ramped up in time. When the voltage reaches a certain value B, the membrane expands suddenly to another stable state C. Note the large difference in the volumes of the two states B and C. When the voltage is ramped down, the membrane shrinks back somewhat, reaching state D at zero voltage.

6. A recipe to achieve giant voltage-induced deformation

As mentioned before, several aspects of the setup of a membrane mounted on a chamber enable the voltage to trigger giant deformation. First, the chamber can be pressurized to place the membrane near the verge of snap-through instability. Second, the instability can be triggered by voltage. Third, the setup can be designed so that the membrane snaps to a stable state without electric breakdown. These aspects are examined in this section by using numerical simulation.

6.1. Placing a membrane near the verge of snap-through instability

When the maximum electric field of the membrane exceeds a certain limit, electric breakdown takes place. The critical state for electrical breakdown is marked by a cross in Fig. 6b. In this case, the breakdown voltage is lower than the voltage needed to trigger the snap-through instability. Consequently, after the voltage triggers the snap, the membrane expands excessively, and suffers electric breakdown before it reaches the stable state C. To facilitate the snap-through expansion without electric breakdown, one can either lower the voltage needed to trigger the snap or raise the voltage for electric breakdown.

To lower the voltage needed to trigger the snap, one may place the membrane nearer the verge of instability by increasing the pressure (Fig. 7). When the pressure is low, such as $pA/\mu H=1.2$ (Fig. 7a and b), an excessively high voltage is required to trigger the snap. Consequently, before the snap the membrane suffers electric breakdown, leading to small voltage-induced deformation.

For a higher pressure of $pA/\mu H=1.5$ (Fig. 7c and d), the initial state of the membrane is closer to the verge of instability. The voltage needed to trigger the snap is lowered, enabling the snap-through expansion prior to electric breakdown. However, during the snap-through expansion, the membrane thins down excessively, and the electric field in the membrane exceeds the breakdown limit before the membrane reaches the stable state.

For an even higher pressure of $pA/\mu H=1.9$ (Fig. 7e and f), a low voltage triggers the snap, enabling the membrane to reach the stable state without electric breakdown. By raising the voltage further, the membrane continues to deform until it reaches breakdown limit.

When the pressure is very high, such as $pA/\mu H=2.0$ (Fig. 7g and h), the snap-through expansion of membrane occurs prior to applying voltage. When the voltage is switched on and ramped up, the membrane deforms somewhat as the voltage increases, until electric breakdown takes place.

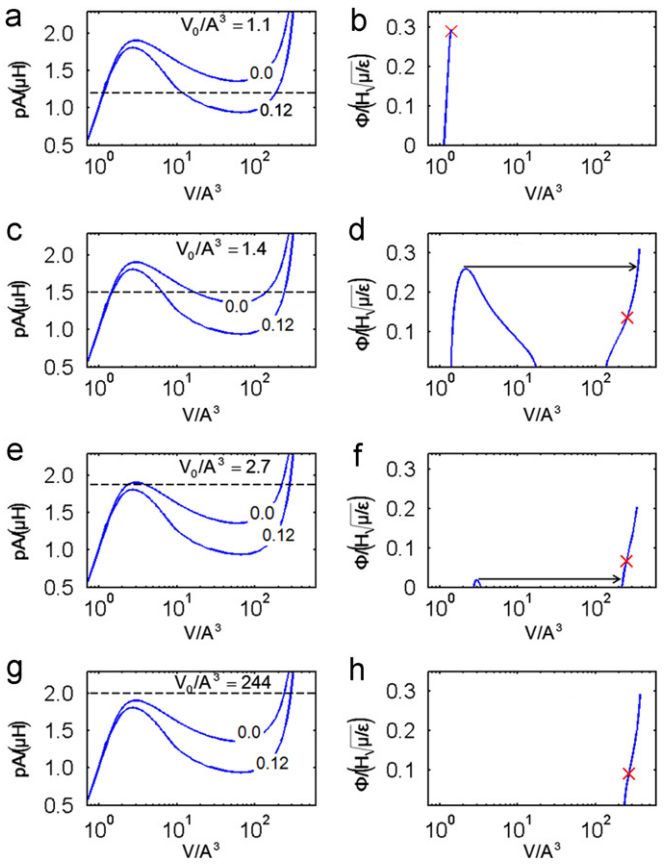

Fig. 7. Numerical results for a membrane actuated at several values of differential pressure.

Also labeled in Fig. 7 are the initial volumes V_0 under the pressurized membranes prior to the application of voltage. Evidently, the membrane can be pushed infinitely close to the verge of instability, and the voltage required to trigger the snap can be infinitesimal. After the snap, the electric field in the membrane is still quite low, and the membrane reaches a stable state of a large volume without electric breakdown. However, preparing the membrane too close to the verge of instability is undesirable; the membrane would snap under disturbance in the environment other than voltage.

6.2. *Bending the snap-through path by using an air chamber of suitable volume*

Instead of pushing the membrane very near the verge of instability, we may restrain the excessive deformation by bending the snap-through path. This can be accomplished by changing the volume of the chamber, V_C. When a membrane is mounted on the chamber, the membrane is flat, and the pressure in the chamber is the same as the atmosphere pressure, p_{atm}. When air is pumped into the chamber through a valve, the membrane is inflated into a balloon of volume V_0, and the pressure in the chamber becomes p_0+p_{atm}. The valve is subsequently closed, fixing the amount of air enclosed by the chamber and the membrane. When the voltage Φ is applied, the volume under the membrane becomes V, and the pressure in the chamber becomes $p+p_{atm}$. We assume the air moves fast enough so that the pressure keeps uniform in the chamber and the balloon. As mentioned before, we restrict our analysis to isothermal processes. (Our experiment, however, may deviate from isothermal processes when the balloon expands suddenly. This deviation is neglected in this paper.) Because the amount of air enclosed by the chamber and the balloon remains unchanged, the ideal-gas law requires that

$$(p+p_{atm})(V+V_C)=(p_0+p_{atm})(V_0+V_C) \tag{24}$$

as the volume of the balloon increases, the pressure p drops. For a chamber of a given volume, the pressure–volume curve of the air (24) is a curve on the pressure–volume plane, representing the snap-through path.

We fix the dimensionless value $p_{atm}/(\mu H/A)=50$ and the initial volume of the balloon $V_0/A^3=2.42$. The pressure–volume curve of the air (the dashed line) intersects with the pressure–volume curves of the membrane at several points, each defining a state of equilibrium (Fig. 8a). These states of equilibrium are shown in the voltage–volume plane (Fig. 8b). The balloon is in state A before the voltage is applied. When the voltage is turned on and ramped up, the balloon expands

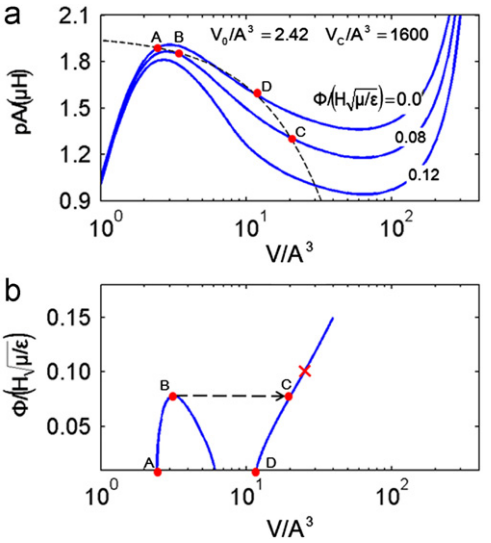

Fig. 8. Numerical results for a membrane mounted on a chamber of volume $V_C/A^3=1600$. The membrane is pressurized to a balloon of initial volume $V_0/A^3=2.42$. (a) Pressure–volume curves of the membrane at several values of voltage. The dashed line is the pressure–volume curve of the air. (b) Voltage–volume curve.

further, and the pressure–volume curves of the balloon lowers. When the voltage reaches 0.08, the pressure–volume curve of the air is tangential to the pressure–volume curve of the balloon at B, and the balloon snaps to state C. As the voltage increases further, the balloon expands further, until it suffers electric breakdown. If the voltage is ramped down from state C, the balloon will shrink back and stay in state D when voltage drops to zero. States A and D are bistable states under no voltage. For a structure of two stable states of equilibrium, one state can be switched to the other by voltage, but voltage is not needed to maintain either state (Wingert et al., 2006). Such a mechanism of actuation eliminates energy dissipation associated with applying a high voltage over a long period of time. In this particular example, one can use voltage to switch the membrane from state A to state D, but cannot use voltage to switch back from state D to state A. One can also design structures to achieve two-way switches (Chouinard and Plante, 2012).

Fig. 9 shows the snap-through paths for membranes mounted on chambers of different volumes. For a small chamber ($V_C/A^3=30$, Fig. 9a and b), the pressure drops steeply as the balloon expands under voltage. Before the membrane snaps, the electric field at the apex of the membrane is already sufficient to cause electric breakdown. Consequently, the membrane fails with small deformation.

For a chamber of volume $V_C/A^3=800$ (Fig. 9c and d), the pressure drops less steeply as the balloon expands under voltage, and the membrane snaps when the voltage reaches a certain level. The deformation after the snap is restrained so that the membrane survives the snap, reaching a stable state without electric breakdown. When the voltage is ramped down, the balloon shrinks, and snaps back at a certain voltage and eventually returns to its initial state. Consequently, as the voltage ramps up and down, the state of the membrane goes through hysteresis. The electromechanical snap-through and snap-back jumps may be used in actuators. A possible advantage would be the option to trigger large changes in shape with small changes in voltage. Furthermore, with less viscoelastic materials such as natural rubber or PDMS, the N-shaped voltage–volume relation could also allow for very fast actuation.

The case of $V_C/A^3=1600$ has been discussed above. For a very large chamber ($V_C/A^3=25{,}000$, Fig. 9g and h), the pressure remains nearly constant after voltage is applied, and the voltage needed to trigger the snap is substantially reduced. The balloon becomes very large; before reaching a stable state, the membrane suffers electric breakdown.

6.3. *Altering voltage-induced deformation by prestretch*

Before being mounted on the chamber, membranes can be prestretched (Fig. 4b). The prestretch can alter the bifurcation diagrams. Fig. 10 shows the experimentally measured pressure–volume curves for membranes of different values of prestretch mounted on a chamber. When the prestretch is $\lambda_0=1$, the pressure–volume curve shows clear peak pressure followed by a large deformation. When the prestretch is $\lambda_0=2$, the peak pressure is less pronounced. When the prestretch is $\lambda_0=3$, the pressure increases monotonically with volume. Consequently, the prestretch can also be used as a parameter to the behavior of the setup. This effect of prestretch is consistent previous experimental observation (Pelrine et al., 2000) and theoretical analysis (Koh et al., 2011b).

Simulations are carried out under several values of prestretch and constant pressure. For a pre-stretch of $\lambda_0=1$, the pressure–volume curves at fixed values of voltage are N-shaped (Fig. 11a). When the voltage triggers the snap, and membrane suffers electric breakdown before reaching the stable state of large volume (Fig. 11b). For a pre-stretch of $\lambda_0=2$,

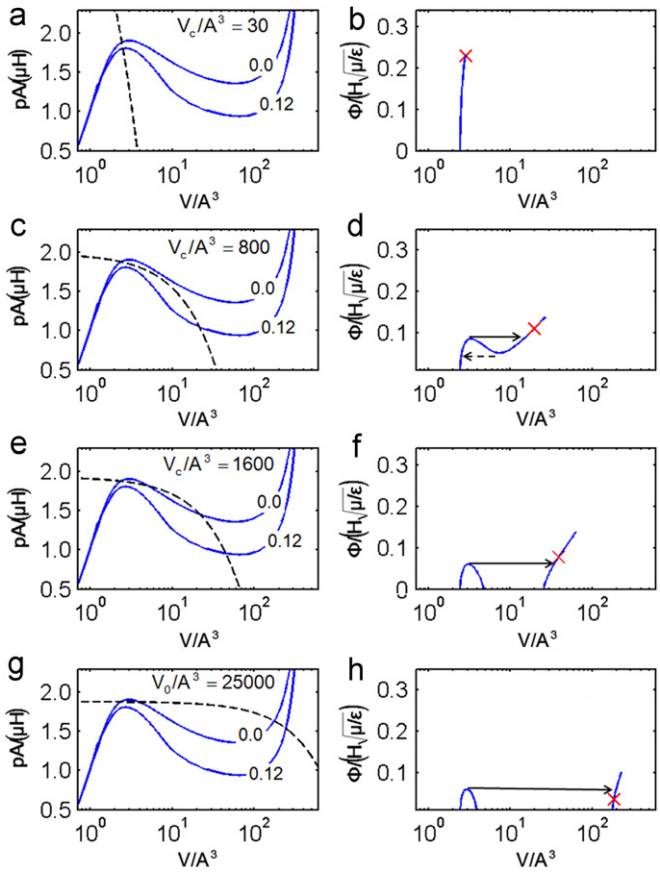

Fig. 9. Numerical results for a membrane mounted on chambers of different volumes.

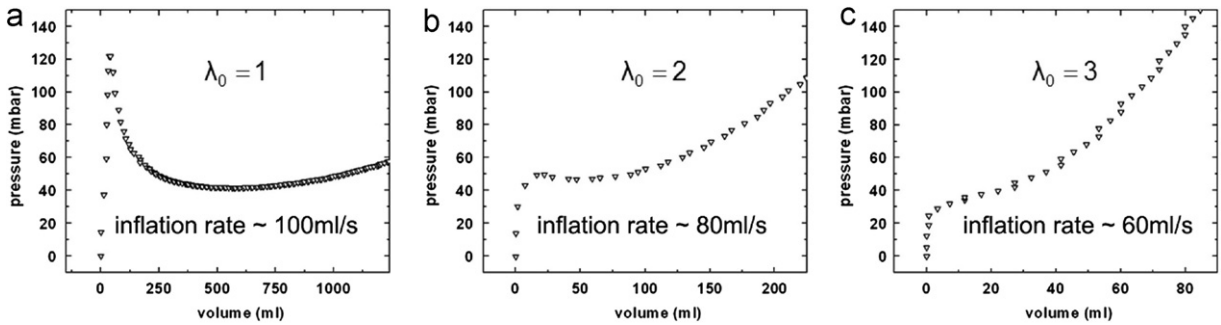

Fig. 10. Experimentally determined pressure–volume curves for membranes of different values of prestretch mounted on a small chamber (0.35 L).

the pressure–volume is essentially monotonic at zero voltage, but becomes N-shaped at a constant value of voltage (Fig. 11c). When voltage is ramped up and down, the membrane undergoes hysteresis, averting electric breakdown (Fig. 11d). For an even larger pre-stretch of $\lambda_0=3$, the pressure–volume curves become monotonic even when voltage is quite large (Fig. 11e). The voltage–volume curve is monotonic (Fig. 11f), a behavior desirable in many applications.

Suitable amount of prestretch can reduce the pressure needed to place the membrane near the verge of instability, enlarge the voltage-induced deformation, and restrain the excessive deformation after the snap.

7. Experiments and discussions

Inspired by the numerical simulations described in Section 6, we conduct the following experiment. A dielectric membrane of acrylic elastomer (3M™VHB™4910), thickness $H=1$ mm, is sandwiched between two carbon-grease electrodes, and mounted without prestretch on a chamber with an opening of radius $A=22.5$ mm. Air is pumped into

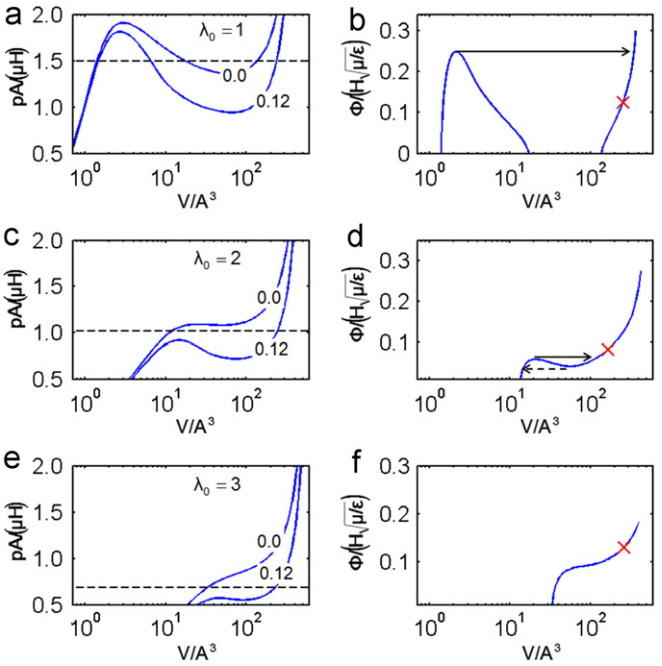

Fig. 11. Numerical results for membranes subject to various values of prestretch.

the chamber through a valve, inflating the membrane into a balloon of volume $V_0=12$ ml and pressure $p_0=19$ mbar. The side view of the balloon is tracked with a video camera, and the recorded images are used to calculate the volume of the balloon, assuming the balloon is axisymmetric. The excess pressure in the chamber is recorded with a pressure sensor (JUMO™ dtrans p30) placed inside the chamber. The balloon is near the verge of the snap-through instability. The valve is subsequently closed to fix the amount of air enclosed by the chamber and the balloon. The voltage is then applied between the two electrodes, and is ramped up and then down in time (Fig. 12a). To ascertain the drastically different types of the voltage–volume curves, we conduct the experiment with chambers of different volumes: 0.35 L, 20 L and 300 L.

For the small chamber of volume 0.35 L, the voltage increases the volume of balloon negligibly, and no snap-through instability is observed (Fig. 12b). As the voltage is ramped up and down, the balloon deforms from A to B and back to C. This behavior corresponds to the type shown in Fig. 9b predicted by the model.

For the chamber of an intermediate volume of 20 L, however, the response to the voltage is drastically different (Fig. 12c). For voltages below the critical level around 4 kV, the volume of the balloon only varies slightly. When the voltage exceeds this value, the balloon expands suddenly, reaching a stable state of a much larger volume. As the voltage is ramped up and then ramped down, the balloon first expands greatly from D to E, and then contracts slightly to F. When the voltage is ramped down to zero, the balloon does not recover its initial volume. This behavior corresponds to the type shown in Fig. 9f predicted by the model.

For the chamber of a large volume of 300 L, the balloon snaps when the voltage reaches a certain level (Fig. 12d). The balloon expands under the same level voltage. The electric field in the membrane intensifies causing electric breakdown before the balloon reaches a stable state. The failure occurs when the voltage is still ramped up, and the experiment is terminated by switching off the voltage. This behavior corresponds to the type shown in Fig. 9h predicted by the model.

Fig. 13 shows the side views and top views of the membrane on the chamber of 20 L at states D and E in Fig. 12. Giant voltage-induced deformation is achieved. We measure the stretch at the top by locating three tracer particles. An average vector–length stretch ratio of 4.23 is measured between the tracer particles, giving an expansion of area of 1692%. This experiment is discussed in more detail in Keplinger et al. (2012). Though no intension is made to optimize the experimental conditions to maximum voltage-induced deformation, the value obtained here is well beyond the previously reported maximum of 380% (Pelrine et al., 2000).

Fig. 14 shows four states of the membrane mounted on the small chamber of volume 0.35 L. Here voltage is ramped up until the membrane fails by electric breakdown. Prior to electric breakdown, a region of the membrane bulges out. The formation of the bulge is captured in detail in supporting videos. Video 1 shows a stereo view (recorded with Trilion QualitySystems ARAMIS) of the process, together with a visualization of in situ pressure and voltage data. Video 2 is a high speed video (recorded with Photron FASTCAM, 2500 frames per second) of the process filmed from the side. Fig. 15 shows a state of the balloon mounted on chamber of the intermediate volume of 20 L. When the voltage is ramped up and kept at 5.5 kV for several minutes, the membrane deforms further and forms wrinkles and clefts. Similar instabilities in dielectric

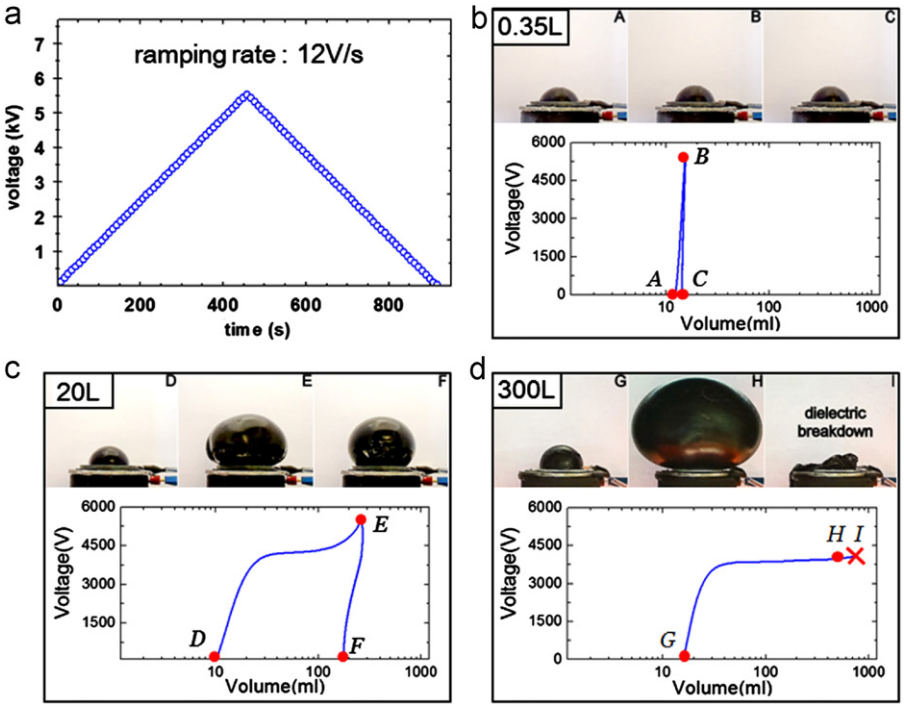

Fig. 12. Experimental observations. (a) Voltage is ramped up and then down in time. (b)–(d) Voltage–volume responses of the balloons mounted on chambers of different volumes.

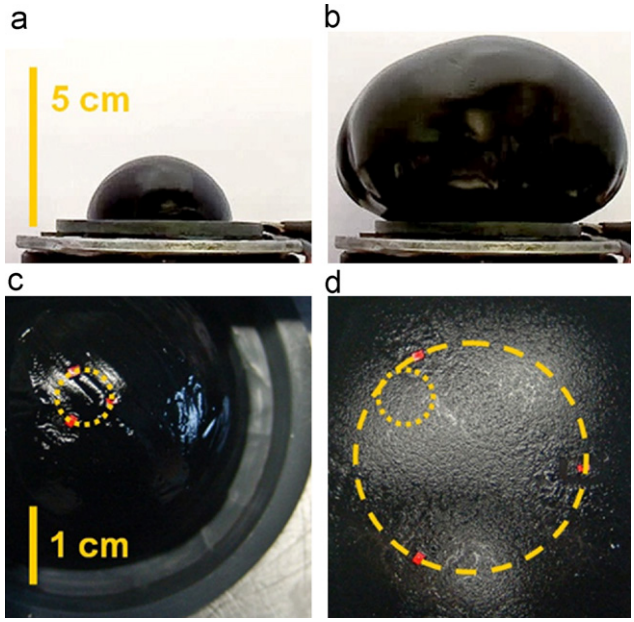

Fig. 13. (a) and (b) Side-views for states D and E of Fig. 12. (c) and (d) The corresponding top-views with tracer particles to measure the area strain.

elastomers have been observed (e.g., Plante and Dubowsky, 2006; Ha et al., 2007), but their systematic study is limited (Huang and Suo, 2012; Zhu et al., 2012). They indicate additional modes of bifurcation and effects of viscoelasticity.

8. Concluding remarks

Dielectric elastomers are susceptible to electromechanical instability. The instability often leads to electric breakdown, but can also be harnessed to achieve giant voltage-induced deformation. We demonstrate this idea with a commonly used

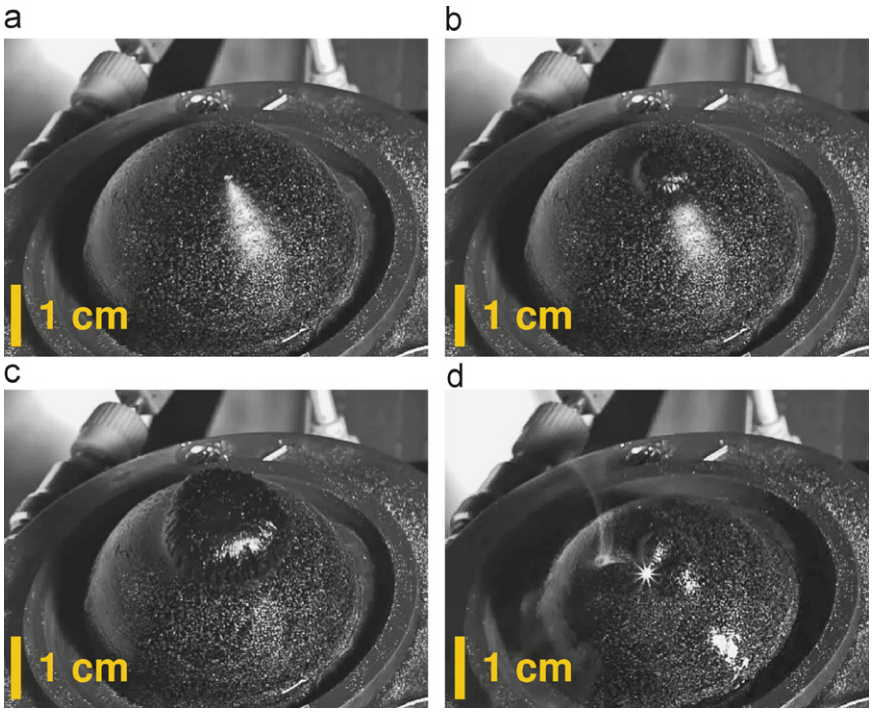

Fig. 14. Small chamber (0.35 L) is used for a membrane without prestretch. Pressure and volume are set to the initial conditions of Fig. 12. Voltage is ramped up like in Fig. 12 until local instability happens. The electric breakdown happens at 8 kV. A region of the membrane bulges out prior to electric breakdown.

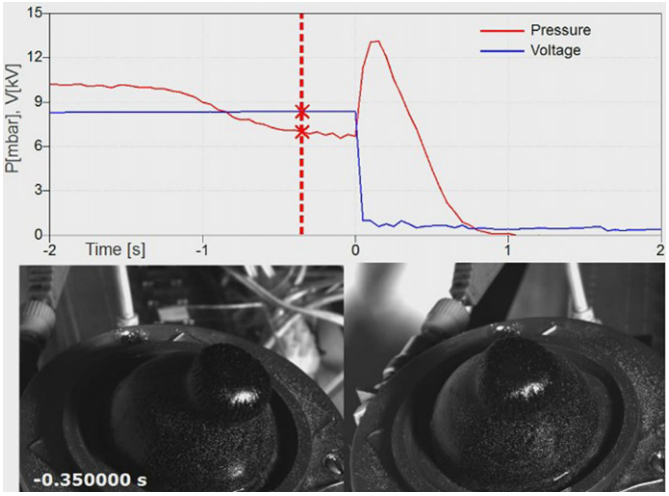

Video 1. A video clip is available online. Supplementary material related to this article can be found online at http://dx.doi.org/10.1016/j.jmps.2012.09.006 The stereo view of the bulge formation (recorded with Trilion QualitySystems ARAMIS) together with a visualization of in-situ pressure and voltage data.

experimental setup—a dielectric membrane mounted on a chamber. The membrane is inflated by pressurizing the chamber, and by applying voltage through the thickness of the membrane. The electromechanical behavior can be dramatically changed by varying the initial pressure in the chamber, the volume of the chamber, and the prestretch of the membrane. To model the experiment, we combine nonlinear electromechanical coupling and kinematics of large axisymmetric deformation. Numerical simulation captures inhomogeneous deformation and maps out bifurcation diagrams. The theoretical prediction has guided us to perform the experiment with suitable values of the parameters, demonstrating record-high voltage-induced deformation. The experiment has also shown phenomena that are beyond the scope of the model. Even for this relatively simple setup, the rich nonlinear coupling enables dramatic changes in the behavior. This work illustrates the importance to combine theory and experiment in exploring complex nonlinear

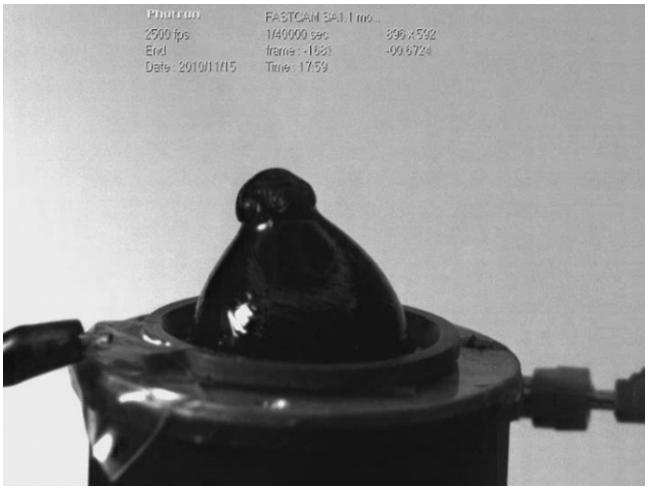

Video 2. A video clip is available online. Supplementary material related to this article can be found online at http://dx.doi.org/10.1016/j.jmps.2012.09.006 High speed video (recorded with Photron FASTCAM, 2500 frames per second) of the bulge formation process filmed from the side.

Fig. 15. The chamber size is 20 L and the membrane is not prestretched. Voltage is ramped up and is then kept at 5.5 kV for several minutes. The membrane forms wrinkles and clefts.

behavior. This work also highlights the potential of harnessing the complex nonlinear behavior to achieve extreme performance. Large voltage-induced deformation is desired for many applications, including soft robots (Shephard et al., 2011), adaptive optics, balloon catheters and Braille displays (Carpi et al., 2010). Snap-through expansion may be used in applications in "polymer intelligence" (O'Brien et al., 2010) as switches or valves. Moreover, for a structure of two stable states of equilibrium, one state can be switched to the other by voltage, but voltage is not needed to maintain either state (Chouinard and Plante, 2012; Wingert et al., 2006). Our results could provide options in designing binary systems.

Acknowledgments

Tiefeng Li acknowledges a two-year visit to Harvard University funded by the China Scholarship Council Foundation and by the School of Engineering and Applied Sciences at Harvard. The work was supported by the National Natural Science Foundation of China (No. 10832009) and the Fundamental Research Funds for the National Universities. The work was also supported by the Austrian Science Fund and by the European Research Council through the Advanced Research Grant SoftMap. The work at Harvard is supported by ARO (W911NF-09-1-0476), DARPA (W911NF-10-1-0113), and MRSEC. The supporting videos and Fig. 14 were produced with the help of Prof. Zoltan Major, who also kindly provided the video equipment.

References

Adkins, J.E, Rivlin, R.S., 1952. Large elastic deformations of isotropic materials. IX. The deformation of thin shells. Philos. Trans. R. Soc. A 244, 505–531.
Alexander, H., 1971. Tensile instability of initially spherical balloons. Int. J. Eng. Sci. 9 (1), 151–160.
Arruda, E.M., Boyce, M., 1993. A three-dimensional constitutive model for the large stretch behavior of rubber elastic materials. J. Mech. Phys. Solids 41, 389–412.
Bertoldi, K., Gei, M., 2011. Instabilities in multilayered soft dielectrics. J. Mech. Phys. Solids 59, 18–42.

Bogen, D.K., McMahon, T.A., 1979. Do cardiac aneurysms blow out? Biophys. J. 27, 301–316.
Boyce, M.C., 1996. Direct comparison of the Gent and the Arruda-Boyce constitutive models of rubber elasticity. Rubber Chem. Technol. 69, 781–785.
Brochu, P., Pei, Q.B., 2010. Advances in dielectric elastomers for actuators and artificial muscles. Macromol. Rapid Commun. 31, 10–36.
Carpi, F., Bauer, S., De Rossi, D., 2010. Stretching dielectric elastomer performance. Science 330, 1759–1760.
Chouinard, P., Plante, J.S, 2012. Bistable antagonistic dielectric elastomer actuators for binary robotics and mechatronics. IEEE/ASME Trans. Mechatron. 17, 857–865.
De Tommasi, D., Puglisi, G., Saccomandi, G., Zurlo, G., 2010. Pull-in and wrinkling instabilities of electroactive dielectric actuators. J. Phys. D 43, 325501.
Diaz-Calleja, R., Riande, E., Sanchis, M.J., 2008. On electromechanical stability of dielectric elastomers. Appl. Phys. Lett. 93, 101902.
Dorfmann, A., Ogden, R.W., 2005. Nonlinear electroelasticity. Acta Mech. 174, 167–183.
Foo, C.C., Cai, S.Q., Koh, S.J.A., Bauer, S., Suo, Z.G., 2012. Model of dissipative dielectric elastomers. J. Appl. Phys. 111, 034102.
Fox, J.W., Goulbourne, N.C., 2008. On the dynamic electromechanical loading of dielectric elastomer membranes. J. Mech. Phys. Solids 56, 2669–2686.
Gent, A.N., 1996. A new constitutive relation for rubber. Rubber Chem. Technol. 69, 59–61.
Goulbourne, N.C., Mockensturm, E.M., Frecker, M.I., 2005. A nonlinear model for dielectric elastomer membranes. ASME J. Appl. Mech. 72, 899–906.
Goulbourne, N.C., Mockensturm, E.M., Frecker, M.I., 2007. Electro-elastomers: large deformation analysis of silicone membranes. Int. J. Solids Struct. 44, 2609–2626.
Ha, S.M., Yuan, W., Pei, Q.B., Pelrine, R., Stanford, S., 2007. Interpenetrating networks of elastomers exhibiting 300% electrically-induced area strain. Smart Mater. Struct. 16, 280–287.
He, T.H., Zhao, X.H., Suo, Z.G., 2009. Dielectric elastomer membranes undergoing inhomogeneous deformation. J. Appl. Phys. 106, 083522.
Hong, W., 2011. Modeling viscoelastic dielectrics. J. Mech. Phys. Solids 59, 637–650.
Huang, R., Suo, Z.G., 2012. Electromechanical phase transition in dielectric elastomers. Proc. R. Soc. A468, 1014–1040.
Huang, J.S., Li, T.F., Foo, C.C., Zhu, J., Clarke, D.R., Suo, Z.G., 2012. Giant, voltage-actuated deformation of a dielectric elastomer under dead load. Appl. Phys. Lett. 100, 041911.
Keplinger, C., Kaltenbrunner, M., Arnold, N., Bauer, S., 2010. Rontgen's electrode-free elastomer actuators without electromechanical pull-in instability. Proc. Natl. Acad. Sci. USA 107 (10), 4505–4510.
Keplinger, C., Li, T.F., Baumgartner, R., Suo, Z.G., Bauer, S., 2012. Harnessing snap-through instability in soft dielectrics to achieve giant voltage-triggered deformation. Soft Matter 8, 285–288.
Klingbeil, W.W., Shield, R.T., 1964. Some numerical investigations in empirical strain energy functions in the large axisymmetric extensions of rubber membranes. Z. Angew. Math. Phys. 15, 608–629.
Kofod, G., Sommer-Larsen, P., Kornbluh, R., Pelrine, R., 2003. Actuation response of polyacrylate dielectric elastomers. J. Intell. Mater. Syst. Struct. 14, 787–793.
Koh, S.J.A., Keplinger, C., Li, T.F., Bauer, S., Suo, Z.G., 2011a. Dielectric elastomer generators: how much energy can be converted. IEEE/ASME Trans. Mechatron. 16, 33–41.
Koh, S.J.A., Li, T.F., Zhou, J.X., Zhao, X.H., Hong, W., Zhu, J., Suo, Z.G., 2011b. Mechanisms of large actuation strain in dielectric elastomers. J. Polym. Sci. B49, 504–515.
Kollosche, M., Zhu, J., Suo, Z.G., Kofod, G., 2012. Complex interplay of nonlinear processes in dielectric elastomers. Phys. Rev. E 85, 051801.
Kornbluh, R.D., Pelrine, R., Prahlad, H., Wong-Foy, A., McCoy, B., Kim, S., Eckerle, J., Low, T., 2012. Dielectric elastomers: stretching the capabilities of energy harvesting. MRS Bull. 37, 246–253.
Leng, J.S., Liu, L.W., Liu, Y.J., Yu, K., Sun, S.H., 2009. Electromechanical stability of dielectric elastomers. Appl. Phys. Lett. 94, 211901.
Li, B., Zhou, J.X., Chen, H.L., 2011. Electromechanical stability in charge-controlled dielectric elastomer actuation. Appl. Phys. Lett. 99, 244101.
Li, B., Chen, H.L., Qiang, J.H., Zhou, J.X., 2012. A model for conditional polarization of the actuation enhancement of a dielectric elastomer. Soft Matter 8, 311–317.
Lochmatter, P., Kovacs, G., Wissler, M., 2007. Characterization of dielectric elastomers based on a visco-hyperelastic film model. Smart Mater. Struct. 135, 748–757.
Lu, T.Q., Huang, J.S., Jordi, C., Kovacs, G., Huang, R., Clarke, D.R., Suo, Z., 2012. Dielectric elastomer actuators under equal-biaxial forces, uniaxial forces, and uniaxial constraint of stiff fibers. Soft Matter 8, 6167–6173.
Ma Z.Y., Jerry I.S., Jar W., Lee., Brian, A.N., 1994. High field electrostrictive response of polymers. J. Polym. Sci. B 32, 2721–2731.
McMeeking, R.M., Landis, C.M., 2005. Electrostatic forces and stored energy for deformable dielectric materials. J. Appl. Mech. 72, 581–590.
Mockensturm, E.M., Goulbourne, N., 2006. Dynamic response of dielectric elastomers. Int. J. Non-Linear Mech. 41, 388–395.
Muller, I., Struchtrup, H., 2002. Inflating a rubber balloon. Math. Mech. Solids 7, 569–577.
Needleman, A., 1977. Inflation of spherical rubber balloons. Int. J. Solids Struct. 13, 409–421.
Norris, A.N., 2008. Comment on 'method to analyze electromechanical instability of dielectric elastomers'. Appl. Phys. Lett. 92, 026101.
O'Brien, B., McKay, T., Calius, E., Xie, S., Anderson, I., 2009. Finite element modelling of dielectric elastomer minimum energy structures. Appl. Phys. A 94, 507–514.
O'Brien, B.M., Calius, E.P., Inamura, T., Xie, S.Q., Anderson, I.A., 2010. Dielectric elastomer switches for smart artificial muscles. Appl. Phys. A 100, 385–389.
Pelrine, R., Kornbluh, R., Joseph, J., 1998. Electrostriction of polymer dielectrics with compliant electrodes as a means of actuation. Sensors Actuators A: Phys. 64, 77–85.
Pelrine, R., Kornbluh, R., Pei, Q.B., Joseph, J., 2000. High-speed electrically actuated elastomers with strain greater than 100%. Science 287, 836–839.
Plante, J.S., Dubowsky, S., 2006. Large-scale failure modes of dielectric elastomer actuators. Int. J. Solids Struct. 43, 7727–7751.
Plante, J.-S., Dubowsky, S., 2007. On the performance mechanisms of dielectric elastomer actuators. Sensors Actuators A 137, 96–109.
Rivlin, R.S., Saunders, D.W., 1951. Large elastic deformations of isotropic materials.7. Experiments on the deformation of rubber. Philos. Trans. R. Soc. A 243, 251–288.
Rosset, S., Niklaus, M., Dubois, P., Shea, H.R, 2009. Large-stroke dielectric elastomer actuators with ion-implanted electrodes. J. Microelectromech. Syst. 18, 1300.
Rudykh, S., Bhattacharya, K., deBotton, G., 2012. Snap-through actuation of thick-wall electroactive balloons. Int. J. Non-Linear Mech. 47, 206–209.
Seydel, R., 2010. Practical Bifurcation and Stability Analysis. Springer, New York.
Shepherd, R.F., Ilievski, F., Choi, W., Morin, S.A., Stokes, A.A., Mazzeo, A.D., Chen, X., Wang, M., Whitesides, G.M., 2011. Multi-gait soft robot. Proc. Natl. Acad. Sci. 108, 20400–20403.
Stark, K.H., Garton, C.G., 1955. Electric strength of irradiated polythene. Nature 176, 1225–1226.
Suo, Z.G., Zhao, X.H., Greene, W.H., 2008. A nonlinear field theory of deformable dielectrics. J. Mech. Phys. Solids 56, 467–486.
Suo, Z.G., 2010. Theory of dielectric elastomers. Acta Mech. Solidia Sin. 23, 549–578.
Trimarco, C., 2009. On the dynamics of electromagnetic bodies. Int. J. Adv. Eng. Sci. Appl. Math. 1, 157–162.
Vu, D.K., Steinmann, P., Possart, G., 2007. Numerical modelling of non-linear electroelasticity. Int. J. Numer. Methods Eng. 70, 685–704.
Wang, H.M., Cai, S.Q., Carpi, F., Suo, Z.G, 2012. Computational model of hydrostatically coupled dielectric elastomer actuators. J. Appl. Mech. 79, 031008.
Wingert, A., Lichter, M.D., Dubowsky, S., 2006. On the design of large degree-of-freedom digital mechatronic devices based on bistable dielectric elastomer actuators. IEEE/ASME Trans. Mechatron. 11, 448–456.
Wissler, M., Mazza, E., 2005a. Modeling of a pre-strained circular actuator made of dielectric elastomers. Sensors Actuators A 120, 184–192.
Wissler, M., Mazza, E., 2005b. Modeling and simulation of dielectric elastomer actuators. Smart Mater. Struct. 14, 1396–1402.
Xu, B.X., Mueller, R., Classen, M., Gross, D., 2010. On electromechanical stability analysis of dielectric elastomer actuators. Appl. Phys. Lett. 97, 162908.
Yong, H.D., He, X.Z., Zhou, Y.H., 2012. Electromechanical instability in anisotropic dielectric elastomers. Int. J. Eng. Sci. 50, 144–150.

Zhao, X.H., Hong, W., Suo, Z.G., 2007. Electromechanical hysteresis and coexistent states in dielectric elastomers. Phys. Rev. B 76, 134113.
Zhao, X.H., Suo, Z.G., 2007. Method to analyze electromechanical stability of dielectric elastomers. Appl. Phys. Lett. 91, 061921.
Zhao, X.H., Suo, Z.G., 2008. Electrostriction in elastic dielectrics undergoing large deformation. J. Appl. Phys. 104, 123530.
Zhao, X.H., Suo, Z.G., 2010. Theory of dielectric elastomers capable of giant deformation of actuation. Phys. Rev. Lett. 104, 178302.
Zhao, X.H., Koh, S.J.A., Suo, Z.G., 2011. Nonequilibrium thermodynamics of dielectric elastomers. Int. J. Appl. Mech. 3, 203–217.
Zhu, J., Cai, S.Q., Suo, Z.G., 2010. Resonant behavior of a membrane of a dielectric elastomer. Int. J. Solids Struct. 47, 3254–3262.
Zhu, J., Kollosche, M., Lu, T.Q., Kofod, G., Suo, Z.G, 2012. Two types of transition to wrinkles in dielectric elastomers. Soft Matter 8, 8840–8846.